RSC Advances

ROYAL SOCIETY OF CHEMISTRY

www.rsc.org/advances

Aqueous-phase hydrodechlorination and further hydrogenation of chlorophenols to cyclohexanone in water over palladium nanoparticles modified dendritic mesoporous silica nanospheres catalyst

Yansheng Liu, Zhengping Dong, Xinlin Li, Xuanduong Le, Wei Zhang and Jiantai Ma**

Gansu Provincial Engineering Laboratory for Chemical Catalysis, College of Chemistry and Chemical Engineering, Lanzhou University, Lanzhou 730000, PR China.

** Corresponding author, E-mail addresses: dongzhp@lzu.edu.cn (Zhengping Dong), majiantai@lzu.edu.cn (Jiantai Ma).*

Tel.: +86 0931 891 2577; Fax: +86 0931 891 2582

Abstract

Dendritic mesoporous silica nanospheres (DMSNs) have been synthesised in this work. The distance of each "arborization" is 7 nm, which plays a role of "pore". Hydrodechlorination (HDC) of 4-chlorophenol (4-CP) as the target compound using Pd modified DMSNs as a catalyst (Pd/DMSNs) is carried out under the condition of sodium hydroxide aqueous solution under atmospheric H_2 pressure, fairly mild conditions for a potential application to treat industrial wastewate. Compared with some supported Pd catalysts, Pd/DMSNs exhibite higher catalytic performance, owing to its particular dendritic structure which can improve mass transfer, increase adsorption–desorption rate of compounds. In this work, the dechlorinate process and further hydrogenation process of 4-CP HDC are both studied under the condition of different amounts of catalyst dosages and temperatures. By analyzing the experiments results, it indicates that the influence factors mentioned above have a strong impact on the selectivity of HDC experiment. In addition, 2-CP, 3-CP, and 2,4-DCP are also tested as the target pollutants in all cases.

1. Introduction:

As important commercial industrial raw materials, chlorophenols (CPs) have been largely mainly employed in different domains, such as manufacture of herbicides, dyes and plant growth regulators, wood, paints, fibers, leather preservatives, as well as disinfectants.[1, 2] However, because of their highly toxic and poorly degradable characters in the wastewater, soil and polluted groundwater, CPs have constituted a particular group of priority toxic chlorinated pollutants listed by the US EPA.[3] Hence, how to dispose CPs into less harmful compound and harmless compound has become a major environmental concern. In order to dispose CPs, a lot of methods have been used, such as oxidative, photocatalytic degradation,[4] thermal combustion, aerobic/anaerobic biodegradation,[5, 6] catalytic reaction based on polymer membrane[7] and reduction dechlorination.[8, 9] In order to achieve destruction/removal efficiencies, the high temperature is necessary in the process of thermal combustion and oxidative treatment of CPs and that an un-ignored possibility of highly toxic dioxins formation in these processes should be concerned. By contrast, the application of a relatively environmental-friendly method, which is biological treatments, is also limited by the toxicity of CPs. These limitations are forcing researchers to develop a more environmentally friendly technique for CPs removal. In the consideration of economic and reactive efficiency, catalytic hydrodechlorination (HDC) is now regarded as a promising technology, since it is suitable for a wide range of chlorinated compounds, mild reaction conditions, and able to facilitate raw material recycle comparing with all

the other alternatives.[10]

In the 1960s, the study of HDC of CPs was initiated, but the first comprehensive report of the liquid phase exhaustive HDC of CPs to phenol over Pd/C only appeared in 1992.[11] From then on, HDC of CPs has been extensively studied. In the literatures, the study directions mainly focused on the structure of the catalyst, reaction media, reaction condition and sources of hydrogen.[12, 13] Till now, supported metal nanocatalysts have been largely studied, such as supported Pd[13-17], Pt[18, 19], Rh[20], Ni[15] and some bimetal alloy catalysts.[21] By comparing the catalytic activity, Pd based catalyst is the best choice for HDC of CPs under the condition of ordinary temperature and atmospheric pressure. In order to develop an efficient Pd based catalyst, multiple supported Pd catalysts have been employed in HDC of CPs, like Pd/activated carbon (AC),[22-24] Pd/Al_2O_3[25] or Pd/zeolites[26, 27] have been studied. As support, Al_2O_3 shows a highly mechanical resistance and a strong interaction with metal NPs, leading to enhanced metal dispersion. But it is very sensitive to HCl that formed upon the reaction, while activated carbons are much more resistant to this compound.[28] So, fibrous spherical dendritic mesoporous silica nanospheres (DMSNs) with 7 nm pore structure come into our sight. As support, DMSNs possesses some features such as high surface area and dendritic mesoporous structure, which offer molecules an easy accessibility through its fibers (as opposed to the traditional use of pores). The dendritic structure can grasp metal NPs and the space between arborizations can improve mass transfer, and increase adsorption–desorption rate of

compounds. These characters make DMSNs an ideal support candidate to form noble metal-based catalysts. Considering its economic, environmental-friendly property, high efficiency and easy-made property, DMSNs supported Pd nanocatalyst (Pd/DMSNs) is designed and employed in HDC of CPs. In addition, Pd/DMSNs nanocatalyst is a promising candidate for various Pd-based catalytic applications.

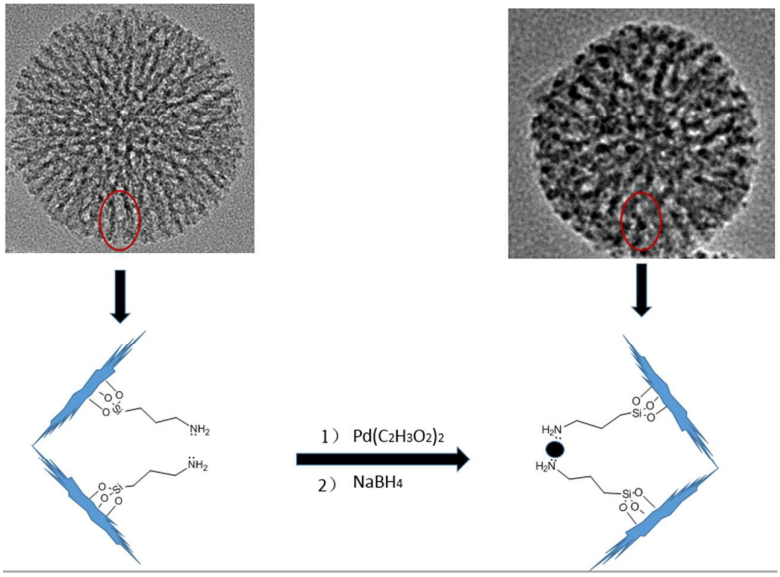

Scheme 1. Preparation of Pd/DMSNs nanocatalyst

2. Experimental

2.1 Materials

Tetraethoxysilane (TOES), Pd(II) acetate, (3-aminopropyl)triethoxysilane (APTES) and hexadecyl trimethyl ammonium chloride (CTAC) are purchased from Aladdin Chemical Co., Ltd. 2-CP, 3-CP, 2,4-DCP and concentrated ammonia aqueous solution are purchased from Lanzhou Aihua Chemical Company. $NaBH_4$ is supplied by

Sinophrm Chemical Reagent Co., Ltd. Oganic solvents used are of analytical grade and did not require further purification.

2.2 Preparation of Pd/DMSNs (dendritic mesoporous silica nanospheres)

DMSNs composite is reported by Dongyuan Zhao.[29] In this work, one generation DMSNs is used as support, and a simple and green method (Scheme 1) has been used. Firstly, DMSNs is functionalized with APTES to obtain DMSNs-NH_2 nano-composites. Secondly, 500 mg of DMSNs-NH_2 nanocomposite were added into a 100 mL round-bottom flask with 108 mg of $Pd(OAc)_2$ and 50 mL of acetonitrile, then ultrasonically dispersed for 30 min and keep stirring for 12 h. Subsequently, the fresh $NaBH_4$ solution (0.3 M, 10 mL) is added dropwise into the abovementioned suspension. The product is isolated by centrifugation and washed several times with deionized water and ethanol, and then dried in a vacuum overnight.

2.3 General procedure for the hydrodechlorination of CPs.

HDC experiments are performed in a three-necked jacketed glass reactor equipped with H_2 supplied. A certain amount of catalyst is placed into the mixed solution of 30 mL solvent, 0.5 mmol of CPs and a certain amount of base under H_2 continuously passed at 45 mL min^{-1}. The reaction maintained for 270 min under vigorous stirring at a certain temperature. The results of the experiments are analysed by Gas chromatography-Mass spectrometry (GC-MS).

2.4 General methods

Transmission electron microscopy (TEM) images are obtained on a Tecnai G2 F30, FEI, USA. The Brunauer–Emmett–Teller (BET) surface area and pore-size distribution are obtained by measuring N_2 adsorption isotherms at 77 K using a TriStar 3020 (Micromeritics). Powder x-ray diffraction (XRD) spectra are obtained by a Rigaku D/max-2400 diffractometer using Cu-Kα radiation in the 2θ range of 0°-80°. X-ray photoelectron spectroscopy (XPS) is recorded on a PHI-5702 and the C1S line at 284.6 eV is used as the binding energy reference. The reaction conversion is estimated by using GC-MS (P.E. AutoSystem XL).

3. Results and Discussion

3.1 Characterization

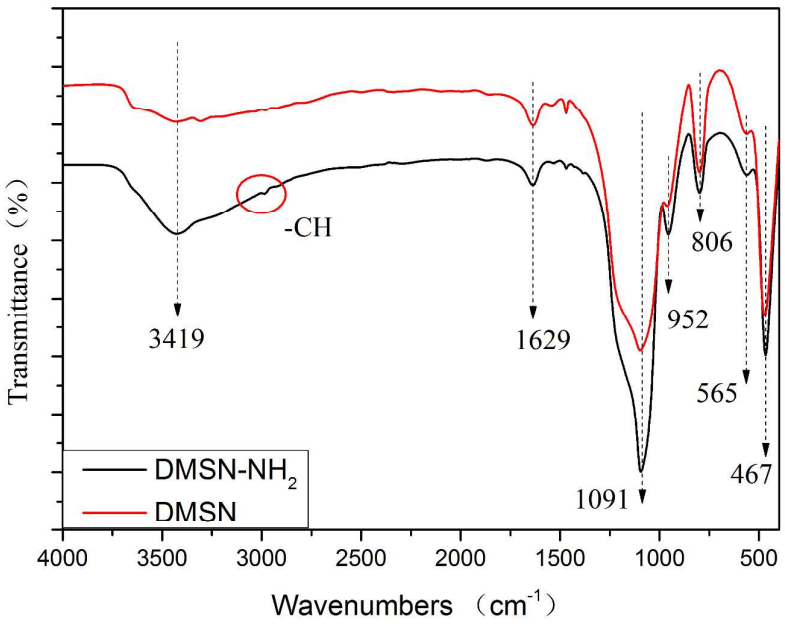

Figure1. FT-IR spectra of DMSN and DMSN-NH_2.

Figure 1 shows the FT-IR spectra of DMSN and DMSN-NH_2. The adsorption peaks at 1091 cm^{-1} and 806 cm^{-1} corresponding to the antisymmetric and symmetric stretching vibrations of Si–O–Si bond in oxygen-silica tetrahedron, respectively. The peak at 467 corresponds to Si–O stretching. The strong peak at 3419 cm^{-1} shows a large number of Si–OH groups proved to be advantageous to the modification of APTES on the DMSN surface by hydrogen bonds. The adsorption peak at 2986 cm^{-1} corresponds to -CH stretching. In the FT-IR spectrum of DMSN-NH_2, the peak around 3419 cm^{-1} represents the adsorption of –OH and –NH_2 groups. The nitrogen, hydrogen, and carbon contents are 1.29%, 1.57%, and 8.98%, measured by the elementary analysis, respectively. The FT-IR spectra and elementary analysis result reveal that the APTES is successfully grafted on the DMSN surface, thus enabling them to act as robust anchors for metal NPs.

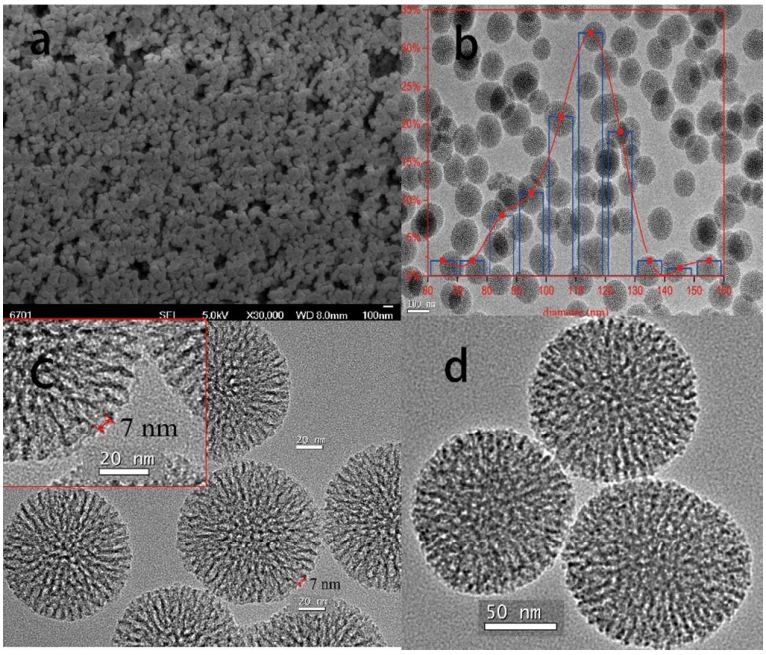

Figure 2. SEM image of DMSNs (a), TEM image of DMSNs (b,c)and Pd/DMSNs (d).

SEM image and TEM image of DMSNs and Pd/DMSNs are presented in Figure 2. As illustrated in Figure 2c, mesoporous silica nanospheres with dendritic structure is presented. The ordered dendritic fibers come from the center of the particle and are distributed uniformly in all directions. Besides, a representative dimension of a pore can be calculated by measuring the distance of two fibers in TEM micrographs, which is about 7 nm (Figure 2c). According to the large-scale TEM image (Figure 2b) of DMSNs, size frequency curve is obtained (*inset of Figure 2b*). From size frequency curve it can be concluded that the particles size of the prepared DMSNs is within the range from 60-160 nm and the mean diameter size is within the range of 90-130 nm. The TEM image of Pd NPs loaded on DMSNs catalyst is shown in Figure 2d. From Figure 2d, it clearly shows that the well-dispersed Pd NPs loads on the internal surface of DMSNs and the calculated Pd NPs diameter is about 4 nm.

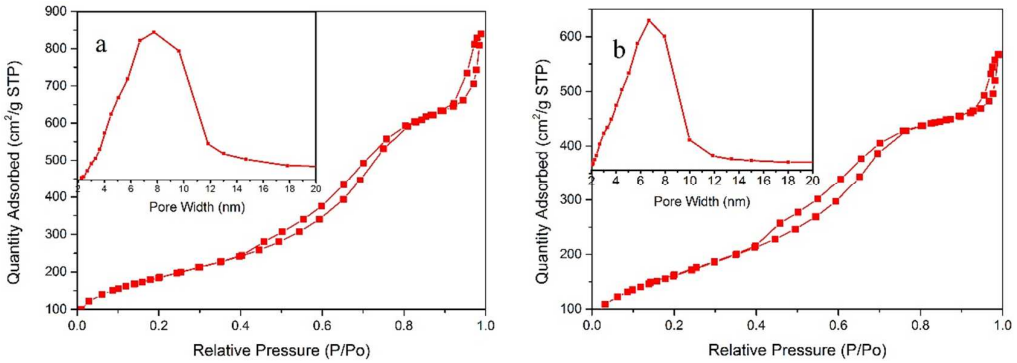

Figure 3. Nitrogen adsorption–desorption isotherms and pore size distribution (*inset*) of DMSNs (a) and Pd/DMSNs (b).

Table 1. Surface area, pore volume and pore size of DMSNs and Pd Pd/DMSNs

Sample	Surface Area (m^2/g)	Pore Volume (cm^3/g)	Pore Size (nm)
DMSNs	664.7	1.30	7.80
Pd/DMSNs	566.7	0.88	6.02

N_2 adsorption-desorption isotherms for the DMSNs and Pd/DMSNs are given in Figure 3. According to the IUPAC classification, the curves of DMSNs and Pd/DMSNs are type IV isotherms with a very sharp capillary condensation stepped at P/P_0 = 0.4–0.8 and H_2-type hysteresis loop, characterizing small-pore mesoporous materials with cylindrical channels. The pore size of DMSNs derived from BJH analysis on the desorption branch is 7.8 nm. The calculated BET surface area and pore volume of DMSNs are 664.7 $m^2\ g^{-1}$ and 1.3 $cm^3\ g^{-1}$, respectively. Compared with DMSNs, the pore size of Pd/DMSNs reduced from 7.8 nm to 6.02 nm, and the pore volume values reduced from 1.3 $cm^3\ g^{-1}$ to 0.88 $cm^3\ g^{-1}$, which owes to the channels dispersed by metal NPs. Besides, surface area of prepared samples reduced from 664.7 $m^2\ g^{-1}$ to 566.7 $m^2\ g^{-1}$ which also indicated that Pd NPs loaded on the DMSNs in some sense.

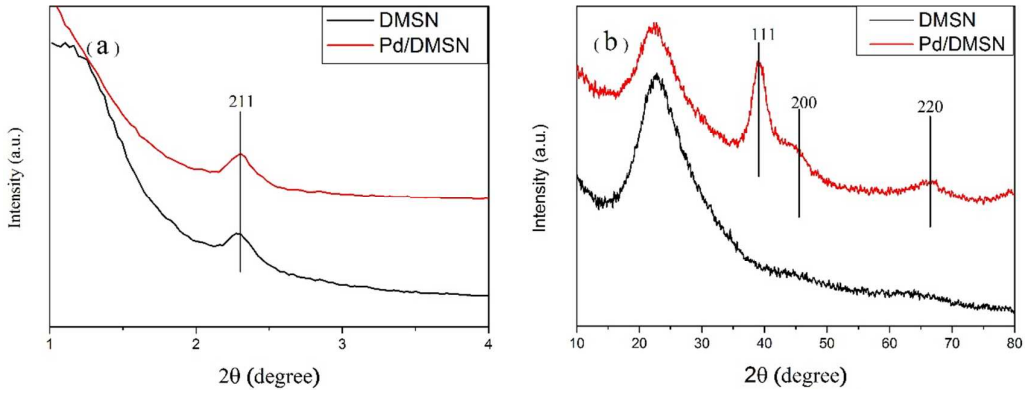

Figure 4. Small-angle (a) and wide-angle (b) XRD patterns of DMSNs and Pd/DMSNs.

XRD patterns of DMSNs and Pd/DMSNs samples are displayed in Figure 4. DMSNs and Pd/DMSNs showed a major diffraction peak at 2θ = 2.3° which corresponds to plane (211) of mesoporous material. The broad peak between 20°–30° corresponds to amorphous silica.[30] The XRD patterns of Pd NPs show three characteristic diffraction peaks at 2θ = 40°, 46° and 68° , corresponding to (111), (200) and (220) respectively. Within the approximation of the Scherrer equation, one would expect a FWHM of 2. 3° 2 theta for the (111) reflection of Pd with an average crystal size of 4.3 nm, which matches with the particles size of Pd NPs calculated by using TEM images.

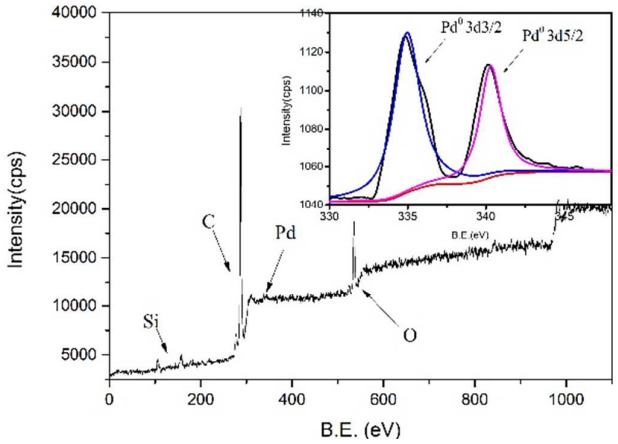

Figure 5. XPS spectra of Pd/DMSN (*inset: high resolution spectrum of Pd 3d*).

Figure 5 presents XPS elemental survey scans of the surface of the Pd/DMSNs catalyst. Peaks corresponding to oxygen, silica and palladium are clearly observed. In the inset figure, $Pd^{(0)}$ binding energy of Pd/DMSNs exhibits two sharp peaks centered at 334.3 eV and 340 eV, which are assigned to Pd $3d_{5/2}$ and Pd $3d_{3/2}$. In addition, no evidence proved the presence of palladium oxide which indicates $Pd(OAc)_2$ is completely reduced to $Pd^{(0)}$ NPs.

3.2 HDC of 4-CP

The catalytic activity of Pd/DMSNs nanocatalyst is established by the HDC of CPs. The HDC of CPs is negligible without catalyst or in the presence of pure DMSN at the same conditions, which shows that the presence of metal NPs is indispensable for high catalytic activity. The 4-CP HDC reaction mechanism is described as below: H_2 adsorbed on the active site of the Pd/DMSNs nanocatalyst is activated into two hydrogen atoms which combined with 4-CP that adsorbed on the surface of the

nanocatalyst. The C-Cl bond of 4-CP is attacked by the active hydrogen atoms to form phenol.[21] Simultaneously, in the process HDC of 4-CP, HCl is formed as a by-product which can poison catalysts. In order to reduce HCl inhibition, NaOH is the best chosen as base to neutralize HCl.[21] With the addition of base, catalyst deactivation is mainly governed by HCl solubility/transport and the nature of the basic species in the catalyst matrix has reported higher HDC rates and enhanced catalyst stability.[31]

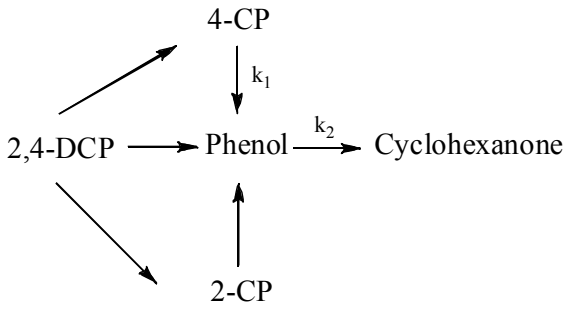

Scheme 2. Schematic of the HDC pathway for CPs.

The HDC pathway is indicated in scheme 2. As Diaz et al.[18] established in a previous work, the route of 4-CP HDC proceeds through a set of series-parallel reactions where 4-CP gives rise to phenol and cyclohexanone (CYC) being this last also produced from phenol hydrogenation. Figure 6 shows the time-dependent concentration of 4-CP and the concentration of the product in the HDC reaction by using Pd/DMSNs nanocatalyst. The investigation of the reaction conditions revealed the maximum conversion of 4-CP in phenol within 270 min. By analyzing the

experiment results, it indicated that under low catalyst dosage (10 mg) and low temperature (20 ℃), only phenol is revealed as dechlorination product. And it should be noticed that, when the conversion value of 4-CP is higher than 80%, a tiny amount of CYC begins to generate. One thing worth mentioning is that, compared with other researchers' works under low Pd dosage and low temperature, the result in this study in agreement with theirs that only phenol is detected as the product. [21, 30, 32-34] When increasing the catalyst dosage from 10 mg to 20 mg and the reaction temperature from 20℃ to 40℃ or 65℃, phenol and further hydrogenation are detected as products in the process of HDC of 4-CP. This result indicated that the amount of activity phase (Pd) and the temperature have a strong effect on the selectivity of experiment.

Table 2. The yield of HDC of CPs catalyzed by Pd/DMSNs.

Reactant	Temperature(℃)	catalyst dosage (mg)	phenol Time (min)/Yield%	CYC Time(min)/Yield%
4-CP	20	10	120/100%	270/2.42%
4-CP	20	20	45/100%	270/4.87%
4-CP	40	20	30/100%	270/18.50%
4-CP	65	20	25/100%	270/29.00%
2-CP	20	10	120/100%	
3-CP	20	10	120/100%	
2,4-DCP	20	10	120/67%	

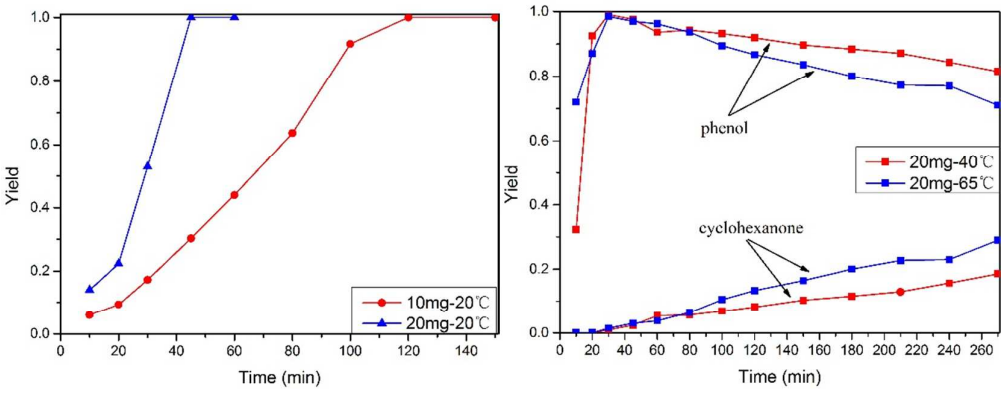

Figure 6. The yield curves of HDC of 4-CP

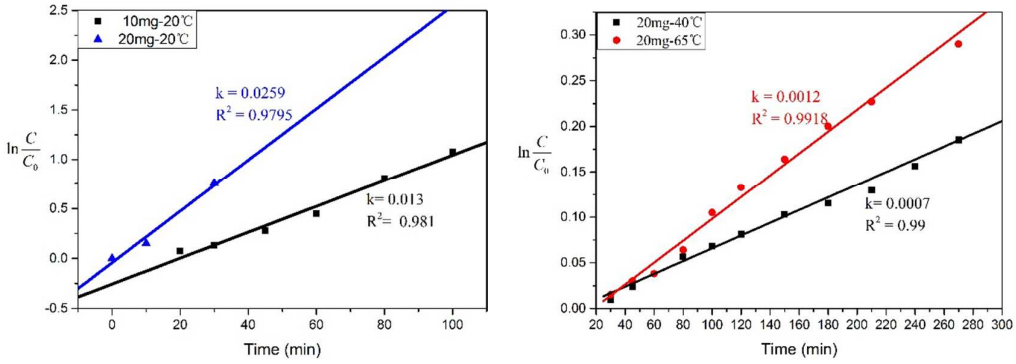

Figure 7. Fitted kinetic rate constants of the 4-CP to phenol (*left*) and phenol to CYC (*right*).

According to the reaction path way(scheme 2), the following rate equations can be written based on the assumption of pseudo-first order kinetics:[35]

$$R_{4\text{-CP}} = \frac{dC_{4-CP}}{dt} = -r_1 = -k_1 C_{4-CP} \quad (1)$$

$$R_{phenol} = \frac{dC_{phenol}}{dt} = r_1 - r_2 = k_1 C_{4-CP} - k_2 C_{phenol} \quad (2)$$

$$R_{CYC} = \frac{dC_{CYC}}{dt} = -r_2 = k_2 C_{phenol} \quad (3)$$

The concentration–time curves for the catalysts at 10.01 wt% metal loading which measured by inductively coupled plasma measurement is fitted to the above equations by a nonlinear regression programme that uses the Marquardt algorithm at the 95% probability level. The kinetic rate constants and the reaction rate constant per unit mass $k_i'=k_i/M_{Pd}$ are calculated and exhibited in Table 3.

Table 3. Fitted kinetic rate constants k_1 for dechlorination process and k_2 for further hydrogenation.

catalyst dosage (mg)	Temperature (℃)	k_1 (min^{-1})	k_1/M_{Pd} (min^{-1} g^{-1})	k_2 (min^{-1})	k_2/M_{Pd} (min^{-1} g^{-1})	R^2
10	20	0.0135	13.5			0.98
20	20	0.0259	13.0			0.98
20	40	0.1300	65.0	0.0007	0.35	0.99
20	65	0.1020	51.0	0.0012	0.60	0.99

In this study, the amount of catalyst dosage (from 10 mg to 20 mg) is doubled under 20 ℃, the dechlorination process kinetic rate constants k_1 increases nearly by one time (from 0.0135 min^{-1} to 0.0259 min^{-1}) and CYC yield value increases nearly to two times (from 2.42% to 4.87%), which indicated that in the reaction system, the relation between the catalytic activity and catalyst dosage is of linear relation. This result also suggests that the amount of catalyst dosage is not an influence factor of 4-CP HDC. Under the condition of 20 mg catalyst dosage, when rising the reaction temperature from 20 ℃ to 40 ℃, both the reaction rate of dechloridation process

and the further hydrogenation process increases. The reaction rate of dechloridation process increases from ~13.2 min^{-1} g^{-1} to 65 min^{-1} g^{-1}, nearly an increase of four times, and the yield of CYC increase from 4.868% to 18.5%, almost increase four times. However, when increasing the reaction temperature from 40 ℃ to 65 ℃, reaction rate k_1 reduces from 65 min^{-1} g^{-1} to 51 min^{-1} g^{-1}, but k_2 increases from 0.35 min^{-1} g^{-1} to 0.6 min^{-1} g^{-1}. This indicated that appropriately increasing reaction temperature can speed up the dechlorination process of 4-CP HDC, but higher temperature will restrain this process. On the contrary, further hydrogenation process does not show a similar tendency. According to this result, it can be concluded that by controlling the catalyst dosage and reaction condition it can selectively degrade CPs to phenol or CYC.

In addition, the condition of large amount of catalyst dosage (100mg) is also studied at 65 ℃. Under the condition mentioned above, 4-CP is completely converted into CYC in 270 min and a very small quantity of cyclohexanol is detected. The HDC of 2-CP, 3-CP and 2,4-DCP are tested and the results are depicted in Table 2. The HDC of 2,4-DCP can proceed in a stepwise and/or concerted fashion with 2-CP and 4-CP as partially dechlorinated products. So, over the same time frame, 67% of 2,4-DCP converts.

The kinetic reaction rate of HDC catalyzed by Pd/Al_2O_3, and Pd/pillared clays catalyst are 3.33 min^{-1} g^{-1} and 7.6 min^{-1} g^{-1}, respectively.[18, 35] As far as reaction rate which is 13.2 min^{-1} g^{-1} at same temperature, Pd/DMSNs exhibited an excellent

catalytic activity performance. By comparing the rate constants for the dechlorination process and further hydrogenation process, the dechlorination proceeds significantly faster than hydrogenation of the resulting primary product, phenol. What's more, kinetic rate constants of dechlorination are much larger than the further hydrogenation of the resulting secondary product, CYC.

According to the kinetic reaction rate of dechlorination process k_1 and further hydrogenation process k_2 at different temperatures within the 20℃–65℃ range in Table 3, the corresponding values of apparent activation energy are calculated by the Arrhenius equation and that values of 61.5 kJ mol^{-1} is obtained for the Pd/DMSNs catalysts. According to literatures having been reported, apparent activation energy of Pd on activated carbon (Pd/AC) ranges from 24.8 kJ mol^{-1} to 47 kJ mol^{-1}.[25, 36, 37] In addition, apparent activation energy of the hydrogenation process is also calculated as 2.28 kJ mol^{-1}.

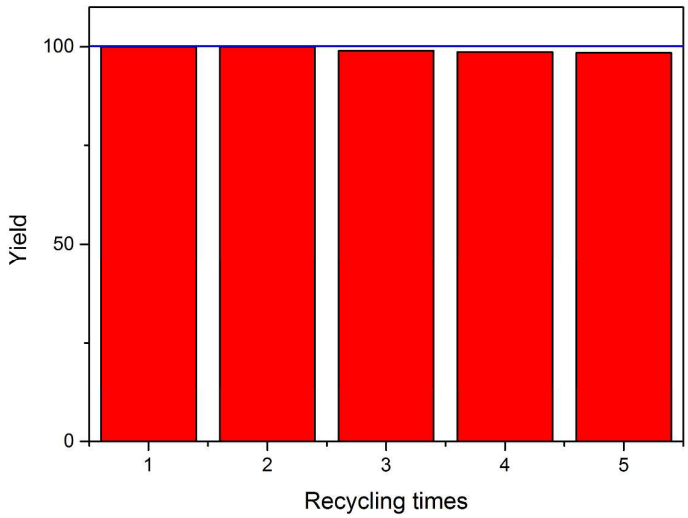

Figure 8. HDC turnover rates of 4-CP HDC over recycled catalyst.

The circulation experiment is performed in a centrifuge tube with H_2 supplied. The catalyst is recovered by centrifugation and simple decantation of liquid products. The catalyst is then washed with deionized water, and used directly for the next cycle of the reaction without further purification. The recoverability and reusability are investigated by the HDC reaction of 4-CP and the results are summarized in Fig. 7. After 5 recycling times, the metal loading of catalyst of 9.89% is measured instead of 10.01% and the catalytic activity of Pd/MSNs shows a slight weakness. This result confirmed the high rate of recyclability of the Pd/DMSNs nanocatalyst and indicated that metal loss is an influence factor for catalytic activity decreasing.

4. Conclusion

In conclusion, Pd/DMSNs catalyst is prepared and the catalytic property of HDC of CPs over the catalyst is investigated. The Pd nanoparticles are fairly active for 4-CP HDC and the further phenol hydrogenation to CYC is observed, which agreed with the study for supported Pd catalysts. Dechlorination process and further hydrogenation HDC of 4-CP can be well described by a simple pseudo-first-order rate equation. The reaction rate constant per unit mass k_1' is 13.2 min^{-1} g^{-1} that is much higher than other Pd supported catalyst under the same reaction temperature (20 ℃). Apparent activation energy values within the range of 61.5 kJ mol^{-1} are obtained for 4-CP disappearance, being a little higher than the reported for supported Pd catalyst, which indicates the important role of the supports on the reaction

pathway. The Pd/DMSNs nanocatalyst acts as a relatively green, economical, and environmental friendly catalyst, and as a promising candidate for various Pd based catalytic applications.

References

1. K. H. Buchel, *Regulatory toxicology and pharmacology : RTP*, 1984, **4**, 174-191.
2. A. I. Tsyganok, I. Yamanaka and K. Otsuka, *Chemosphere*, 1999, **39**, 1819-1831.
3. Q. Wen, T. Yang, S. Wang, Y. Chen, L. Cong and Y. Qu, *J Hazard Mater*, 2013, **244-245**, 743-749.
4. M. P. Ormad, J. L. Ovelleiro and J. Kiwi, *Appl. Catal. B: Environ.*, 2001, **32**, 157-166.
5. G. Buitron, M. E. Schoeb, L. Moreno-Andrade and J. A. Moreno, *Water Res.*, 2005, **39**, 1015-1024.
6. P. S. Majumder and S. K. Gupta, *Bioresour. Technol.*, 2008, **99**, 4169-4177.
7. D. Fritsch, K. Kuhr, K. Mackenzie and F. D. Kopinke, *Catal. Today*, 2003, **82**, 105-118.
8. Y. Han, W. Li, M. Zhang and K. Tao, *Chemosphere*, 2008, **72**, 53-58.
9. W. Zhang, X. Quan, J. Wang, Z. Zhang and S. Chen, *Chemosphere*, 2006, **65**, 58-64.
10. G. S. Pozan and I. Boz, *J Hazard Mater*, 2006, **136**, 917-921.
11. J. B. Hoke, E. N. Balko and G. A. Gramiccioni, *Abstracts Of Papers Of the American Chemical Society*, 1992, **203**, 200-ENVR.
12. H. M. Roy, C. M. Wai, T. Yuan, J. K. Kim and W. D. Marshall, *Appl. Catal. A: Gen.*, 2004, **271**, 137-143.

13. F. D. Kopinke, K. Mackenzie, R. Koehler and A. Georgi, *Appl. Catal. A: Gen.*, 2004, **271**, 119-128.

14. L. Calvo, M. A. Gilarranz, J. A. Casas, A. F. Mohedano and J. J. Rodriguez, *Ind. Eng. Chem. Res.*, 2005, **44**, 6661-6667.

15. L. Calvo, M. A. Gilarranz, J. A. Casas, A. F. Mohedano and J. J. Rodriguez, *Appl. Catal. B: Environ.*, 2008, **78**, 259-266.

16. M. A. Lillo-Ródenas, J. Juan-Juan, D. Cazorla-Amorós and A. Linares-Solano, *Carbon*, 2004, **42**, 1371-1375.

17. G. Yuan and M. A. Keane, *Appl. Catal. B: Environ.*, 2004, **52**, 301-314.

18. E. Diaz, J. A. Casas, A. F. Mohedano, L. Calvo, M. A. Gilarranz and J. J. Rodriguez, *Ind. Eng. Chem. Res.*, 2008, **47**, 3840-3846.

19. J. Halasz, S. Meszaros and I. Hannus, *React. Kinet. Catal. Lett.*, 2006, **87**, 359-365.

20. G. Yuan and M. A. Keane, *Catal. Commun.*, 2003, **4**, 195-201.

21. Z. Dong, X. Le, C. Dong, W. Zhang, X. Li and J. Ma, *Appl. Catal. B: Environ.*, 2015, **162**, 372-380.

22. M. A. Keane, *J. Chem. Technol. Biotechnol.*, 2005, **80**, 1211-1222.

23. G. S. Pozan and I. Boz, *J. Hazard. Mater.*, 2006, **136**, 917-921.

24. G. Yuan and M. A. Keane, *Chem. Eng. Sci.*, 2003, **58**, 257-267.

25. G. Yuan and M. A. Keane, *Catal. Today*, 2003, **88**, 27-36.

26. R. F. Howe, *Appl. Catal. A: Gen.*, 2004, **271**, 3-11.

27. A. Santos, P. Yustos, A. Quintanilla, S. Rodriguez and F. Garcia-Ochoa, *Appl. Catal. B: Environ.*, 2002, **39**, 97-113.

28. Z. M. de Pedro, E. Diaz, A. F. Mohedano, J. A. Casas and J. J. Rodriguez, *Appl. Catal. B: Environ.*, 2011, **103**, 128-135.

29. D. Shen, J. Yang, X. Li, L. Zhou, R. Zhang, W. Li, L. Chen, R. Wang, F. Zhang and D. Zhao, *Nano Lett.*, 2014, **14**, 923-932.

30. X. Le, Z. Dong, X. Li, W. Zhang, M. Le and J. Ma, *Catal. Commun.*, 2015, **59**, 21-25.

31. G. Yuan and M. A. Keane, *Ind. Eng. Chem. Res.*, 2007, **46**, 705-715.

32. X. Le, Z. Dong, W. Zhang, X. Li and J. Ma, *J. Mol. Catal. A: Chem.*, 2014, **395**, 58-65.

33. X. Le, Z. Dong, Y. Liu, Z. Jin, T.-D. Huy, M. Le and J. Ma, *J. Mater. Chem. A*, 2014, **2**, 19696-19706.

34. H. Deng, G. Fan and Y. Wang, *Synthesis And Reactivity In Inorganic Metal-Organic And Nano-Metal Chemistry*, 2014, **44**, 1306-1311.

35. C. B. Molina, A. H. Pizarro, J. A. Casas and J. J. Rodriguez, *Appl. Catal. B: Environ.*, 2014, **148**, 330-338.

36. Y. Shindler, Y. Matatov-Meytal and M. Sheintuch, *Ind. Eng. Chem. Res.*, 2001, **40**, 3301-3308.

37. J. A. C. Elena Dı´az, A´ ngel F. Mohedano, Luisa Calvo, Miguel A. Gilarranz, and Juan J. Rodrı´guez, *Ind. Eng. Chem. Res.*, 2009, **48**, 3351–3358.